Acta Biochim Biophys Sin 2014, 46: 802–809 | © The Author 2014. Published by ABBS Editorial Office in association with Oxford University Press on behalf of the Institute of Biochemistry and Cell Biology, Shanghai Institutes for Biological Sciences, Chinese Academy of Sciences. DOI: 10.1093/abbs/gmu063.
Advance Access Publication 25 July 2014

Short Communication

The S28H mutation on mNeptune generates a brighter near-infrared monomeric fluorescent protein with improved quantum yield and pH-stability

Zhao-Yang Li[1,2], Dian-Bing Wang[3], Zhi-Ping Zhang[1], Li-Jun Bi[3], Zong-Qiang Cui[1], Jiao-Yu Deng[1], and Xian-En Zhang[2,3]*

[1]State Key Laboratory of Virology, Wuhan Institute of Virology, Chinese Academy of Sciences, Wuhan 430071, China
[2]University of Chinese Academy of Sciences, Beijing 100049, China
[3]National Laboratory of Biomacromolecules, Institute of Biophysics, Chinese Academy of Sciences, Beijing 100101, China
*Correspondence address. Tel/Fax: +86-10-64888148; E-mail: zhangxe@sun5.ibp.ac.cn

For living deep-tissue imaging, the optical window favorable for light penetration is in near-infrared wavelengths, which requires fluorescent proteins with emission spectra in the near-infrared region. Here, we report that a single mutant Ser28His of mNeptune with a near-infrared (≥650 nm) emission maxima of 652 nm is found to improve the brightness, photostability, and pH stability when compared with its parental protein mNeptune, while it remains as a monomer, demonstrating that there is still plenty of room to improve the performance of the existing near infrared fluorescence proteins by directed evolution.

Keywords near-infrared; mNeptune; brightness; photostability; deep-tissue imaging

Received: April 14, 2014 Accepted: May 14, 2014

Introduction

Fluorescent proteins (FPs) provide unique opportunities for noninvasive labeling and tracking specific proteins in living organisms in real time. Many GFP-like mutants with a wide range of emission spectrums had been constructed by mutagenesis for multiple purposes. In recent years, one of the most attractive applications is deep optical imaging in mammalian tissues or whole body, which requires near-infrared (NIR) fluorescent probes. In the so-called NIR 'Optical Window' (from 650 to 900 nm) favorable for the visualization in living tissues, mammalian tissues are more transparent to light. Because, in this optical window, the combined absorption of the main photon absorbers (melanin and hemoglobin) within the visual spectrum in living tissues is minimal and the intensity of light scattering caused by animal tissues drops off as the wavelength increases [1]. Several FPs whose emission maxima reach the 650 nm barrier have been developed, such as HcRed [2], mPlum [3], AQ143 [4], mNeptune [5], TagRFP657 [6], and eqFP650 [7]. The first three were earlier reported FPs with the emission spectrum in the far-red or near-infrared region, and the latter three were recently reported brighter FPs, among which eqFP650 is known to be the brightest. Up to now, the maximum emission wavelength of FPs has broken through the barrier of 670 nm, such as the variants eqFP670 [7] and TagRFP675 [8], although their quantum yields are relatively lower. For living deep-tissue imaging, a FP should have a long-emission wavelength with higher quantum yield and molar extinction coefficient. Besides, it should be in a true monomeric structure in solution when used as a labeling tag of a target protein through fusion technology, which is required for correct targeting and localization of fused constructs in living tissues.

We selected mNeptune (excitation peak/emission peak at 600 nm/650 nm) which inherit the brightness advantage of its precursor mKate [9], as the initiation protein to carry out directed evolution, due to its long-emission wavelength and preferable monomeric property among those FPs mentioned above. In the current study, 11 pairs of degenerate primers were used to introduce saturated mutations on the neighboring amino acid sites around the chromophore. Finally, two variants with improved brightness, L13T and S28H, were screened out from the mutation libraries by a site-directed saturation mutation method. Among them, only the single mutant S28H maintains the maxima fluorescence emission >650 nm. Compared with its precursor, mNeptune_S28H (substitution of serine with histidine) possesses the maximum emission wavelength of 652 nm while retains the same monomeric characteristic as that of mNeptune.

Materials and Methods

Plasmid construction

The complementary DNA of FPs, eqFP650, mNeptune and mNeptune_S28H, were cloned into the *Bam*HI/*Sac*I sites of the vector pQE30 (Qiagen, Hilden, Germany).

Mutagenesis and screening

Site-directed random mutation methods were used as previously described [10]. Degenerative primers were employed

to introduce mutations at the neighboring residue sites around the chromophore by overlapping polymerase chain reaction (PCR). To construct mutation libraries, plasmids containing the mutant genes of FPs were transformed into chemically competent *Escherichia coli* strain TG1 or XL1 Blue strain (Invitrogen, Carlsbad, USA). Then, these strains were incubated overnight at 37°C on LB agar plates and then stored at room temperature for 2 days. The plates with fluorescent colonies were first screened for transmitted color by visual inspection. Among all the fluorescent colonies on the plates, the colonies appearing blue color were marked on the bottom of the plates, and were further screened for the bright colonies by a fluorescent stereomicroscope Nikon SMZ 1500 equipped with 550–615 nm excitation filter and 635–685 nm emission filter (Nikon, Tokyo, Japan). Then, the bright colonies, screened out from thousands of colonies, were first cultured in 2 ml LB/ampicillin medium in the 96-deep well plates at 37°C for 24 h, and then were stored at 4°C until the cells appear blue or purple color. Subsequently, the cell pellets were re-suspended in phosphate buffered saline (PBS) buffer (pH 7.4) after centrifugation, and the OD_{600} values and the fluorescence emission intensities at the maximum emission were measured by a Synergy H1 microplate reader. For this screening, *E. coli* cells transformed with the expression plasmid of pQE30-mNeptune were used as controls. By normalizing the maximum fluorescence emission intensities with the OD_{600} values, the brightness of all mutant cells and the control cells was finally quantified. By comparing the normalized brightness of mutant cells with that of the control cells, mutant clones with improved brightness were chosen for the subsequent experiments.

Protein expression and purification

eqFP650, mNeptune, and mNeptune_S28H were expressed in XL1 Blue strain. The bacterial cultures were grown overnight at 37°C and further incubated at 25°C for 12 h according to previous methods [11]. Cultures were collected by centrifugation, and then the cell pellets were resuspended in the binding buffer (20 mM Tris–HCl, 500 mM NaCl, 20 mM imidazole, pH 8.0) and lysed by sonication. The recombinant proteins were purified using an Ni-NTA His-Bind resin (GE Healthcare, Bethesda, USA), followed by a gel filtration step using a Superdex-200 size exclusion column (GE Healthcare). The proteins were stored in PBS for further analysis.

Gel filtration assays

Gel filtration analysis of mNeptune_S28H, mNeptune, and eqFP650 (~3–4 mg/ml) in PBS (pH 7.4) was performed using a Superdex 200 10/300 GL column (GE Healthcare).

Spectroscopic characterization

Absorption spectra of FPs were recorded by a PerkinElmer LAMBDA 25 UV/Vis Spectrophotometer (Perkin Elmer, Waltham, USA). A PerkinElmer LS55 fluorescence spectrophotometer equipped with a red sensitive photomultiplier tube (Hamamatsu Photonics, Hamamatsu, Japan) was used for measuring their excitation/emission spectra. Molar extinction coefficients were quantified by mature RFP chromophore concentration [12]. Briefly, FPs were alkali-denatured with an equal volume of 0.2 M NaOH, under which the RFP chromophores of FPs completely were converted to GFP-like chromophores with an extinction coefficient of 44,000 M^{-1} cm^{-1} [13]. Absorption spectra of native and alkali-denatured proteins were measured. On the basis of the absorption of denatured proteins, molar extinction coefficients for the native state were estimated. To accurately measure the quantum yields, proteins were first diluted in PBS (pH 7.4) with UV absorption values in the range of 0.01–0.05. Fluorescence intensity of the mutant FP was compared with that of mNeptune (quantum yield 0.20).

The pH studies and pK_a measurements

In pH titration assays, FPs were dissolved in a series of buffers in the range from pH 3.0 to 11.0 (200 mM Na_2HPO4, 100 mM citric acid for pH 3.0–7.0, 50 mM Tris–HCl for pH 7.5–9.0, and 200 mM glycine, 200 mM NaOH for pH 9.5–11.0). Equal volumes (200 μl) of the above FP solutions with a concentration of 20 μM were analyzed with a Synergy H1 plate reader in Costar UV transparent 96-well plates for the absorption spectrums. The pK_a values of FPs were taken as the pH value where the absorption or the deprotonation ratio of chromophore reached 50% of the maximum.

Maturation kinetics

E. coli M15/pREP4 cells (Qiagen) were transformed with pQE30 plasmids containing mNeptune, mNeptune_S28H, and eqFP650 genes. Clones from each transformation were used to inoculate a 5-ml LB starter culture, which was grown to an OD_{600} of 0.5. Those starter cultures were each diluted 1 : 50 in 100 ml of fresh LB in 500 ml baffled flask, and shaken at 200 rpm at 37°C. After 3 h, a pulse of gene expression was induced with 1 mM isopropyl β-D-1-thiogalactopyranoside. A chase was initiated after 20 min by inhibiting protein synthesis with 170 mg/ml chloramphenicol and 50 mg/ml tetracycline. At designated time points, 200 μl aliquots were removed from the continuously shaking cultures, and red fluorescence (590 nm excitation, 650 nm emission) was immediately measured using a Synergy H1 fluorescent microplate reader. When red fluorescence was fully matured, the FPs would exhibit the maximum fluorescence intensities. The maximum fluorescence intensities at this time were normalized to 100%. The curves were fitted out according to the percentages of red fluorescence at various time points and sigmoidal function. Maturation times $t_{one\text{-}half}$ were defined as the time point at which the fluorescence reached the half of the maximum fluorescence intensities.

Photobleaching measurements

Aqueous droplets of FPs in PBS solution were mixed with mineral oil. After sufficient vibration using Vortex-Genie 2 (Scientific Industries, Bohemia, USA), microdroplets of FPs were prepared with the size of 5–10 μm to guarantee all FPs under the same irradiation conditions. Photobleaching experiments were carried out using an Olympus IX81 inverted microscope (Olympus, Tokyo, Japan) equipped with standard 561-nm laser light source and 60 × 1.4 NA oil immersion lens. The FP microdroplets surrounded by mineral oil were continuously illuminated for 10–15 min, and images were collected every 0.5 s. Averaged fluorescence signals of FP microdroplets from three independent experiments were quantified using PerkinElmer Volocity 5.3 software. At time zero, the fluorescence signals were normalized to 100%. Photobleaching half-life time was defined as the time point at which the signal dropped to 50% of its initial value.

Results

The variant mNeptune_S28H exhibits improved brightness, photostability, and pH stability

Starting from the wild-type mNeptune, all mutations made in this study were designed to produce amino acid residue replacement surrounding the chromophore that is held by 11 β-strands and were predicted to influence its spectrum properties. Thirty amino acid sites were selected to make mutations. They are Met11, Leu13, and Met15 on β1-strand, Ser28, and Gly30 on β2-strand, Gln39, Gly41, and Ile43 on β3-strand, Phe88, Trp90, and Arg92 on β4-strand, Gln106, and Thr108 on β5-strand, Leu115, Tyr117, and Val119 on β6-strand, Trp140, Glu141, and Ala142 on β7-strand, Cys158, Asp159, and Met160 on β8-strand, Leu174, Thr176, and Tyr178 on β9-strand, Arg197, Arg198, Leu199 on β10-strand, Gln213, Glu215 on β11-strand, respectively. A degenerative primer was designed for each strand so that two or three residues would be randomly replaced by other amino acids at every PCR (**Table 1**). We also used a combination of several primer sets to introduce random combinatorial mutations at several selected sites simultaneously.

To screen out a brighter FP with a longer-emission wavelength, plates of *E. coli* cells transformed with mutagenized plasmid DNAs were used for the preliminary screening of mutants with improved brightness under a fluorescent stereomicroscope. The colonies appearing blue color in ambient lighting on the plates were first labeled, because the colonies exhibiting blue color demonstrated that the colonies perhaps retained a long-emission wavelength similar to that of mNeptune. After the bacteria colonies were screened by visual inspection, the labeled blue colonies continued to be screened for fluorescence using a fluorescent stereomicroscope (Nikon SMZ 1500). In this process, the CCD camera

Table 1. The selected sites of mutation and the primers used for saturation site-directed mutations

	Mutation sites	Degenerative primers
β-1 strand	Met11, Leu13, Met15	5′ TAAGGAGAACATGCAC**NNN**AAG**NNN**TAC**NNN**GAGGGCACCGTGAACAAC 3′
		5′ GTTCACGGTGCCCTC**NNN**GTA**NNN**CTT**NNN**GTGCATGTTCTCCTTA 3′
β-2 strand	Ser28, Gly30	5′ ACCACTTCAAGTGCACA**NNN**GAG**NNN**GAAGGCAAGCCCTAC 3′
		5′ GTAGGGCTTGCCTTC**NNN**CTC**NNN**TGTGCACTTGAAGTGGT 3′
β-3 strand	Gln39, Gly41, Ile43	5′ CCCTACGAGGGCACC**NNN**ACC**NNN**AGA**NNN**AAGGTGGTCGAGGGCGGCCCTCTC 3′
		5′ GCCCTCGACCACCTT**NNN**TCT**NNN**GGT**NNN**GGTGCCCTCGTAGGGCTTG 3′
β-4 strand	Phe88, Trp90, Arg92	5′ CAGTCCTTCCCTGAGGGC**NNN**ACA**NNN**GAG**NNN**GTCACCACATACGAA 3′
		5′ TTCGTATGTGGTGAC**NNN**CTC**NNN**TGT**NNN**GCCCTCAGGGAAGGACTG 3′
β-5 strand	Gln106, Thr108	5′ GCGTGCTGACCGCTACC**NNN**GAC**NNN**AGCCTCCAGGACGGCTGC 3′
		5′ CAGCCGTCCTGGAGGCT**NNN**GTC**NNN**GGTAGCGGTCAGCACGC 3′
β-6 strand	Leu115, Tyr117, Val119	5′ AGCCTCCAGGACGGCTGC**NNN**ATC**NNN**AAC**NNN**AAGATCAGAGGGGTGAA 3′
		5′ TTCACCCCTCTGATCTT**NNN**GTT**NNN**GAT**NNN**GCAGCCGTCCTGGAGGCT 3′
β-7 strand	Trp140, Glu141, Ala142	5′ GCAGAAGAAAACACTCGGC**NNNNNNNNN**TCCACCGAGACGCTGTACC 3′
		5′ GGTACAGCGTCTCGGTGGA**NNNNNNNNN**GCCGAGTGTTTTCTTCTGC 3′
β-8 strand	Cys158, Asp159, Met160	5′ ACGGCGGCCTGGAAGGCAGA**NNNNNNNNN**GCCCTGAAGCTCGTGGG 3′
		5′ CCCACGAGCTTCAGGGC**NNNNNNNNN**TCTGCCTTCCAGGCCGCCGT 3′
β-9 strand	Leu174, Thr176, Tyr178	5′ GGGGCCACCTGATCTGCAAC**NNN**AAG**NNN**ACA**NNN**AGATCCAAGAAACCCGCTAA 3′
		5′ TTAGCGGGTTTCTTGGATCT**NNN**TGT**NNN**CTT**NNN**GTTGCAGATCAGGTGGCCCC 3′
β-10 strand	Arg197, Arg198, Leu199	5′ CGGCGTCTACTTTGTGGAC**NNNNNNNNN**GAAAGAATCAAGGAGGCCGAC 3′
		5′ GTCGGCCTCCTTGATTCTTTC**NNNNNNNNN**GTCCACAAAGTAGACGCC 3′
β-11 strand	Gln213, Glu215	5′ CAATGAGACCTACGTCGAG**NNN**CAC**NNN**GTGGCTGTGGCCAGATAC 3′
		5′ GTATCTGGCCACAGCCAC**NNN**GTG**NNN**CTCGACGTAGGTCTCATTG 3′

equipped on the fluorescent stereomicroscope helped to distinguish the bright colonies from thousands of colonies. After continuous mutation and selection, only two variants with improved brightness, L13T and S28H, were finally screened out from the mutation libraries by fluorescent microplate reader. The mutant L13T exhibits ~1.2-fold higher brightness than mNeptune, but this mutation caused a blue shift of peak emission to 640 nm. Therefore, we did not further determine more spectral properties about this mutant. Spectral analysis by microplate reader showed that only the colony with single mutant S28H retained the maximum emission similar to that of mNeptune, with an emission peak of ~655 nm. Meanwhile, we also found that the colonies transformed with mNeptune_S28H expression plasmids appeared blue color on the second day after the transformation experiment, while the control colonies with mNeptune expression plasmids appeared blue color on the first day after the transformation experiment. Thus, the maturation time of mNeptune_S28H may be slower than that of mNeptune. We characterized the mNeptune_S28H and compared its properties with those of mNeptune. The main characteristics are summarized in **Table 2**. The excitation and emission spectrums were accurately scanned by a fluorescent spectrophotometer at physiological pH (PBS buffer at pH 7.4). The results showed that mNeptune_S28H exhibited excitation and emission peaks at 590 and 652 nm, respectively (**Fig. 1A**).

To investigate the effect of S28H mutation on the brightness of protein, we decided to make a comparison of the brightness of mNeptune with its variant S28H. The molar extinction coefficients and quantum yields of these two proteins were determined under the same conditions. Their molar extinction coefficients were measured using an alkali denaturation method [12,13]. The quantum yield of mNeptune_S28H was obtained using mNeptune (0.20) as a reference. At the same excitation wavelength of 590 nm and under the same scanning conditions, the emission

Table 2. Comparison of the characteristics of mNeptune, mNeptune_S28H, and eqFP650*

FP	E_x/E_m (nm)[a]	E_{mol} (M^{-1} cm^{-1})[d]	QY[e]	B^f_{EGFP}, %	pK_a	Photobleaching half-life time (s)	Oligomeric state	$t_{one\text{-}half}$ for maturation at 37°C (h)
mNeptune	600/650[b]	67,000[b]	0.20[b]	42.1[b]	5.4[b]	ND[b]	Monomer	1.9
	600/655	68,000		42.8	5.2	38		
mNeptune_S28H	590/652	70,000	0.25	55.0	5.0	51	Monomer	1.6
eqFP650	592/650[c]	65,000[c]	0.24[c]	49.1[c]	5.7[c]	67[c]	Dimmer	0.7
	590/650	64,000	0.20	40.3	5.6	130		

*All data presented here were from the current experiments with exception of [b] and [c].
[a]Maximum excitation and emission wavelength.
[b]Data from [5]. ND, not determined.
[c]Data from [7].
[d]Molar extinction coefficient.
[e]Quantum yield.
[f]Brightness relative to EGFP (the product of quantum yield and molar extinction coefficient compared with the brightness of EGFP) (53, 000 M^{-1} cm^{-1} × 0.6) [14].

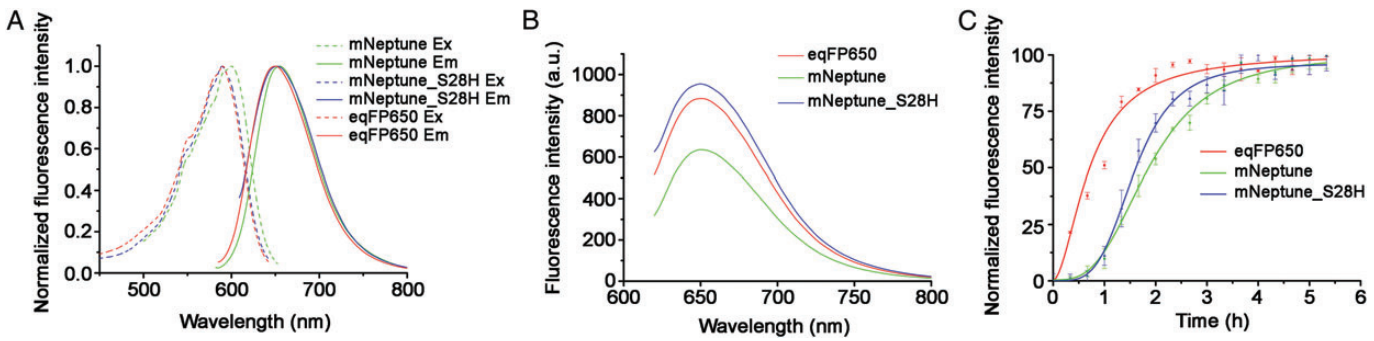

Figure 1. Spectral characteristics and maturation kinetics of FPs (A) Fluorescence excitation (dashed line) and emission (solid line) spectra of three FPs. mNeptune (green line), mNeptune_S28H (blue line) and eqFP650 (red line). (B) The emission spectra of three diluted proteins mNeptune, mNeptune_S28H, and eqFP650 in the range of 620−800 nm were scanned using the same excitation wavelength of 590 nm. (C) Kinetics of red fluorescence maturation for mNeptune (green circles), mNeptune_S28H (blue triangles) and eqFP650 (red squares). Mean of triplicate measurements are shown. Error bars represent standard error of the mean. The curves are fitted out according to the percentages of red fluorescence at various time points and sigmoidal function.

spectrums of mNeptune and mNeptune_S28H in the range of 620–800 nm were recorded using a fluorescence spectrophotometer (**Fig. 1B**). Finally, the results demonstrated that mNeptune_S28H was characterized by a slightly higher molar extinction coefficient of 70,000 M^{-1} cm^{-1} compared with 68,000 M^{-1} cm^{-1} of mNeptune (**Table 2**), and also by a higher fluorescence quantum yield of 0.25 compared with 0.20 of mNeptune (**Table 2**), resulting in ~1.3-fold brighter fluorescence.

To study the effect of S28H mutation on the maturation time of FP, we performed maturation kinetics determination on mNeptune and its variant S28H respectively. The results showed that mNeptune_S28H exhibited a slightly faster maturation with maturation $t_{one\text{-}half}$ of 1.6 h than mNeptune (a half maturation time of 1.9 h) at 37°C (**Fig. 1C**, **Table 2**).

Moreover, FPs used in long-term imaging studies also need to exhibit a high level of photostability. In order to study the influence of S28H mutation on protein photostability, we performed photobleaching experiments on mNeptune and mNeptune_S28H under the same measurement conditions. The photobleaching experiments were conducted using a laser scanning confocal microscope. The results showed that mNeptune_S28H was more photostable than mNeptune, with a longer photobleaching half-life time of 51 s, compared with 38 s of mNeptune (**Fig. 2C**, **Table 2**).

In addition to brightness and photostability, the pH stability is also a key characteristic which determines the use potential of FP in different pH environments. To investigate the effect of pH on the absorbance spectra of proteins, a series of buffers with different pH gradients were prepared. mNeptune and mNeptune_S28H dissolved in PBS (pH 7.4) were diluted to 20 μM, respectively, with these buffers, and the absorbance spectra from 300 to 700 nm were

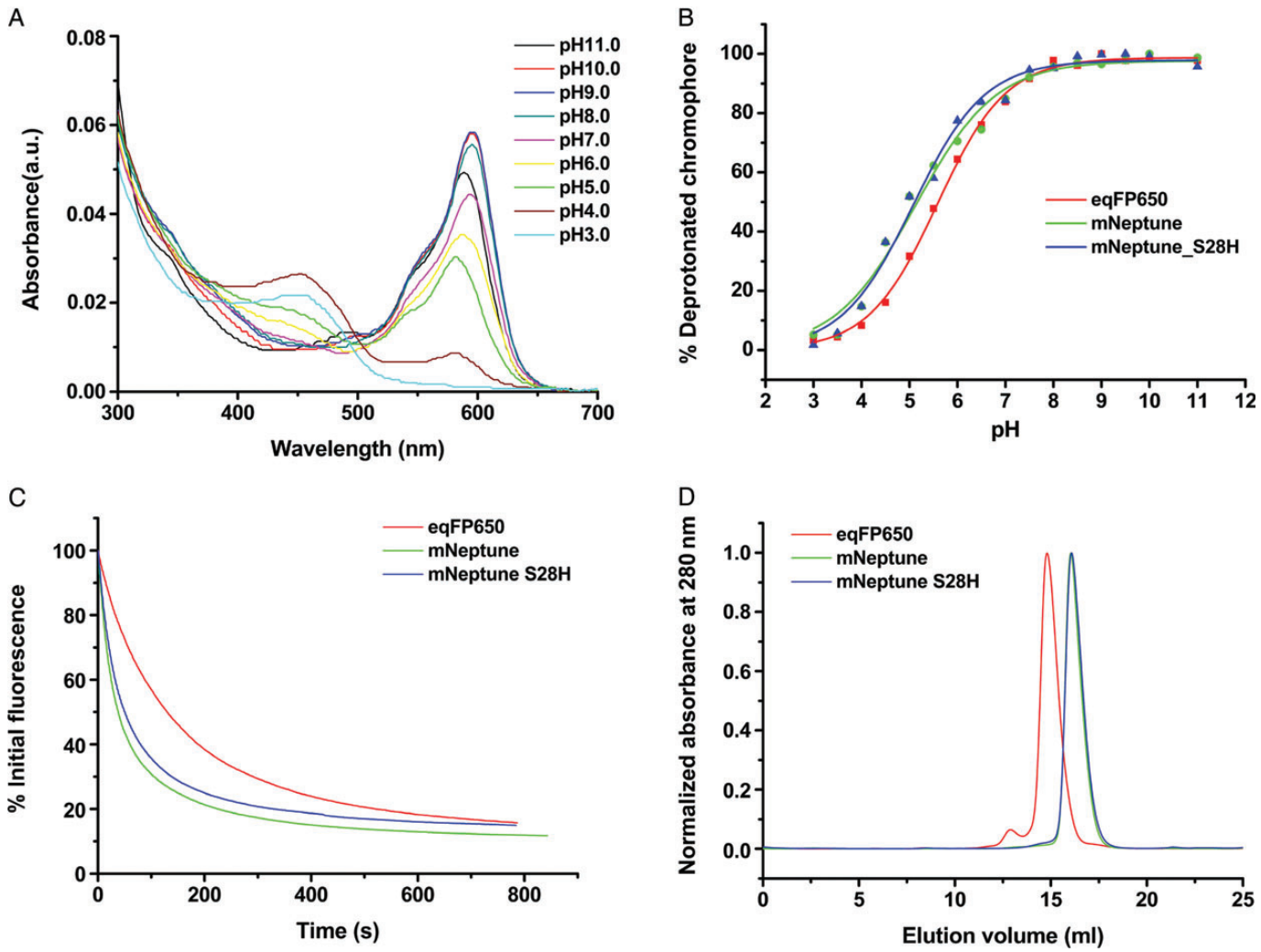

Figure 2. Physical and chemical properties of FPs (A) Photobleaching assays of mNeptune (green solid line), mNeptune_S28H (blue solid line), and eqFP650 (red solid line) were performed using a laser scan confocal microscopy. (B) Gel filtration analysis of mNeptune_S28H (blue solid line) was performed with a Superdex 200 column. The elution volumes of mNeptune (monomer, green solid line) and eqFP650 (dimer, red solid line) were used as controls. (C) The absorbance spectra of mNeptune_S28H in buffers at pH 3.0–11.0. (D) The deprotonated chromophore percentage curves of FPs at different pH levels. mNeptune (green solid line), mNeptune_S28H (blue solid line), and eqFP650 (red solid line).

immediately recorded by Synergy H1 microplate reader (**Fig. 2A**). At different pH levels, the values of absorption peaks represent different deprotonation levels of chromophore. The deprotonation ratio of chromophore at pH 10.0 was set to be 100%, because the chromophore at this high pH level is almost completely in the anion state. The peak values at various pH gradients were converted into corresponding deprotonation ratios. According to Henderson–Hasselbalch equation and various deprontonation ratios at different pH levels, the curves of pH-dependence chromophore deprontonation about mNeptune_S28H and mNeptune were fitted out respectively (**Fig. 2B**). The results showed that mNeptune_S28H exhibited slightly higher pH stability, with a pK_a of 5.0, compared with 5.4 of mNeptune (**Table 2**).

Comparison of the characteristics of mNeptune_S28H and eqFP650

According to the characteristics of mNeptune_S28H measured in this study, we found that the molar extinction coefficient and quantum yield of mNeptune_S28H are apparently higher than those of eqFP650 (molar extinction coefficient is 65,000 M^{-1} cm^{-1}, and quantum yield is 0.24) (**Table 2**). So the brightness of mNeptune_S28H should be ~1.1-fold than that of eqFP650. To find out whether mNeptune_S28H is brighter than eqFP650, we characterized eqFP650 under the same measurement conditions as mNeptune_S28H. The spectral analysis showed that eqFP650 had fluorescence excitation and emission maxima at 590 and 650 nm, respectively. As expected, eqFP650 was characterized by a slightly lower molar extinction (64,000 M^{-1} cm^{-1}) and also by a lower fluorescence quantum yield (0.20) (**Table 2**). According to our measurements, we found that the brightness of the variant mNeptune_S28H was ~40% higher than that of eqFP650. Although the photostability of mNeptune_S28H, with a photobleaching half-life time of 51 s far shorter than 130 s of eqFP650 (**Table 2**), is not as good as that of eqFP650 (**Fig. 2C**), gel filtration analysis showed that the elution volumes of mNeptune_S28H and its parental protein mNeptune were nearly the same, suggesting that mNeptune_S28H still remains as a monomer compared with the known dimeric characteristic of eqFP650 (**Fig. 2D**).

Discussion

Brightness of FPs reflects the capabilities of the chromophores to absorb light (described by the molar extinction coefficient) and to re-emit photons (described by the quantum yield). Due to the given physical size of the chromophore, the molar extinction coefficient is usually constant within a particular FP spectral class [15]. Thus, increasing the quantum yield plays a key role in the course of enhancing the brightness of FPs. The most representative examples occur in a series of cyan fluorescent protein (CFP) variants with brightness enhanced, such as Cerulean [16], SCFP3A [17], mTurquoise [18], and mCerulean3 [19]. From the crystal structures of these reported proteins, scientists found that limiting the conformation fluctuations of amino acid side chains around the chromophore could make the chromophore tightly packed in the β-barrel, and strengthening hydrogen-bond interaction between the chromophore and its neighboring amino acids could rigidify the whole environment surrounding the chromophore [20]. As a result, the chromophore vibrations in the excited state are reduced, resulting in the decrease of non-radiative energy decay. When the chromophore is excited by light, the energy of excitation light is converted into the energy of fluorescence emission as much as possible, leading to higher quantum yield and brightness.

Due to the stronger hydrogen-bond interactions between the chromophore and its surrounding amino acids, two recently reported FPs, mNeptune2.5 and mCardinal, were found to have improved brightness and redshift in excitation and emission, when compared with their common precursor mNeptune [21]. It was shown that mutations in two key amino acid sites play a decisive role in the improvement of spectral characteristics. In mNeptune2.5, two key mutations S28H and G41N result in the enhancement of brightness. In mCardinal, two mutations S28T and G41Q lead to the formation of the stronger hydrogen-bond interactions with the acylimine of chromophore than that of its precursor, which leads to the redshift of excitation and emission spectrums. At the same time, these strengthened hydrogen-bond interactions also provide additional stabilization of the excited state of chromophore in mCardinal and help retain similar brightness with mNeptune.

Compared with the two sites between mNeptune2.5 and mCardinal, the most significant difference lies in the mutation of Ser28. mNeptune2.5 carries S28H mutation, while mCardinal has S28T mutation. Owning to a larger side chain of His than that of Thr, the distance between Residue 28 and the acylimine of chromophore in mNeptune2.5 will be evidently shorter than that of mCardinal, which possibly result in the formation of a stronger hydrogen bond between Residue 28 and the acylimine of chromophore. Therefore, we estimate that single mutant S28H should be brighter than single mutant S28T without the impact of other mutations. In addition to Residue 28, G41Q mutation in mCardinal is the key leading to spectral redshift due to a hydrogen-bond interaction between the side chain amide nitrogen of Gln41 and the chromophore acylimine oxygen. The same mutation has also been studied in another homologous FP TagRFP675 [8]. Because Asn has an analogous side chain structure with Gln, G41N mutation in mNeptune2.5 might also play an important role in the spectral redshift. Thus, we supposed that S28H mutation in mNeptune2.5 may be the main reason for the improved brightness.

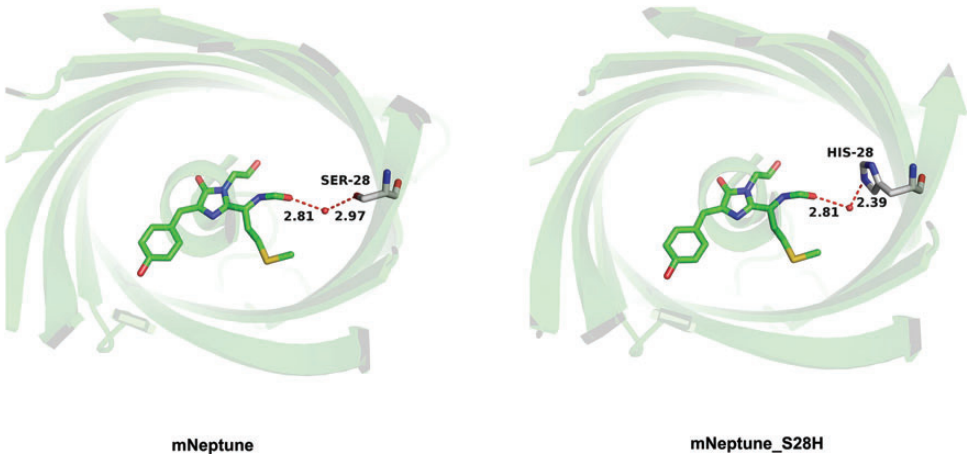

Figure 3. Simulation of the hydrogen-bond interactions between FPs chromophore and its adjacent amino acid at residue position 28 using PyMol software mNeptune and Ser28 (left), mNeptune_S28H and His 28 (right).

When we found that the single mutation S28H in mNeptune could cause a series of significant changes in spectral performance, the same variation was reported by Chu J *et al.* [21]. Nevertheless, we provided a detailed analysis of spectroscopic properties. These two independent findings came to the same conclusion that the mutation S28H can cause the improvement of brightness. And we found that the most prominent feature was its increase of the quantum yield. We speculated that the side chain bulk imidazole group of Histidine was introduced into the vicinity of chromophore, resulting in the reduction of free space around the chromophore in the variant mNeptune_S28H. As a result, the chromophore is packed more tightly. Meanwhile, simulating mutation analysis by PyMol software showed that the distance of hydrogen bond between His28 and the chromophore acylimine group may be shortened after mutation (**Fig. 3**), leading to the enhancement of the hydrogen-bond interactions between them. Due to the above two reasons, the vibrations of chromophore in the excited state may be reduced, resulting in the decrease of non-radiative energy decay. In a word, more dense space packing around the chromophore and stronger hydrogen-bond interactions provide a more rigid environment for chromophore matrix [22,23], which limits non-radiative decay of its excited-state and thus favors the improvement of fluorescence.

On the other hand, the variant mNeptune_S28H with an emission peak of 652 nm still retained a long-emission wavelength similar to mNeptune. From the crystal structure of mNeptune (PDB code: 3IP2), the water-mediated hydrogen-bond interaction between the side chain of Ser28 and the chromophore acylimine group was shown, which may be the reason for the red shift of emission wavelength [5]. Considering that the maximum emission wavelength of mNeptune_S28H is also $>$650 nm, we speculate that similar hydrogen-bond interactions between Residue 28 and the chromophore acylimine group may exist in this mutant as those in mNeptune.

In summary, for living deep-tissue imaging experiments, high reporter expression and high brightness of FPs are usually required. Meanwhile, the true monomeric property of FP is also required, because it will contribute to correct targeting and localization of fused constructs in living tissues. The variant mNeptune_S28H constructed in this study, with one amino acid replacement in its parental protein mNeptune, produced the highest brightness among the reported near-infrared fluorescence emission proteins, and had higher photostability compared with mNeptune while remained a monomeric structure, demonstrating that there is still plenty of room to improve the performance of the existing near-infrared fluorescence proteins by directed evolution.

Acknowledgements

The authors thank Mr. Xu-De Wang (Wuhan Institute of Virology, CAS) for kindly providing the valuable suggestions and guidance on protein experiments, and Mr. Ding Gao (Wuhan Institute of Virology, CAS) for his assistance in the protein photobleaching experiments and related analysis.

Funding

D.-W. was supported by the National High Technology Research and Development Program ("863"Program) of China (2011AA02A114, 2012AA022206). X.Z. was supported by the Chinese Academy of Sciences and the National laboratory of Macrobiomolecules.

References

1. Weissleder R. A clearer vision for *in vivo* imaging. Nat Biotechnol 2001, 19: 316–317.
2. Gurskaya NG, Fradkov AF, Terskikh A, Matz MV, Labas YA, Martynov VI and Yanushevich YG, *et al*. GFP-like chromoproteins as a source of far-red fluorescent proteins. FEBS Lett 2001, 507: 16–20.
3. Wang L, Jackson WC, Steinbach PA and Tsien RY. Evolution of new non-antibody proteins via iterative somatic hypermutation. Proc Natl Acad Sci USA 2004, 101: 16745–16749.

4. Shkrob MA, Yanushevich YG, Chudakov DM, Gurskaya NG, Labas YA, Poponov SY and Mudrik NN, *et al*. Far-red fluorescent proteins evolved from a blue chromoprotein from Actinia equina. Biochem J 2005, 392: 649–654.
5. Lin MZ, McKeown MR, Ng HL, Aguilera TA, Shaner NC, Campbell RE and Adams SR, *et al*. Autofluorescent proteins with excitation in the optical window for intravital imaging in mammals. Chem Biol 2009, 16: 1169–1179.
6. Morozova KS, Piatkevich KD, Gould TJ, Zhang J, Bewersdorf J and Verkhusha VV. Far-red fluorescent protein excitable with red lasers for flow cytometry and superresolution STED nanoscopy. Biophys J 2010, 99: L13–L15.
7. Shcherbo D, Shemiakina II, Ryabova AV, Luker KE, Schmidt BT, Souslova EA and Gorodnicheva TV, *et al*. Near-infrared fluorescent proteins. Nat Methods 2010, 7: 827–829.
8. Piatkevich KD, Malashkevich VN, Morozova KS, Nemkovich NA, Almo SC and Verkhusha VV. Extended Stokes shift in fluorescent proteins: chromophore–protein interactions in a near-infrared TagRFP675 variant. Sci Rep 2013, 3: 1847.
9. Pletnev S, Shcherbo D, Chudakov DM, Pletneva N, Merzlyak EM, Wlodawer A and Dauter Z, *et al*. A crystallographic study of bright far-red fluorescent protein mKate reveals pH-induced *cis–trans* isomerization of the chromophore. J Biol Chem 2008, 283: 28980–28987.
10. Sawano A and Miyawaki A. Directed evolution of green fluorescent protein by a new versatile PCR strategy for site-directed and semi-random mutagenesis. Nucleic Acids Res 2000, 28: E78.
11. Shcherbo D, Murphy C, Ermakova G, Solovieva E, Chepurnykh T, Shcheglov A and Verkhusha V, *et al*. Far-red fluorescent tags for protein imaging in living tissues. Biochem J 2009, 418: 567–574.
12. Gross LA, Baird GS, Hoffman RC, Baldridge KK and Tsien RY. The structure of the chromophore within DsRed, a red fluorescent protein from coral. Proc Natl Acad Sci USA 2000, 97: 11990–11995.
13. Ward WW. Biochemical and physical properties of green fluorescent protein. In Chalfie M and Kain SR (eds). Methods of biochemical analysis, volume 47, green fluorescent protein: properties, applications and protocols. 2nd ed. USA: John Wiley & Sons 2005: 39–65.
14. Bindels DS, Goedhart J, Hink MA, van Weeren L, Joosen L and Gadella TW, Jr. Optimization of fluorescent proteins. In Engelborghs Y and Visser AJ (eds). Methods in molecular biology, volume 1076, fluorescence spectroscopy and microscopy: methods and protocols. Germany: Springer 2014: 371–417.
15. Rizzo MA, Springer GH, Granada B and Piston DW. An improved cyan fluorescent protein variant useful for FRET. Nat Biotechnol 2004, 22: 445–449.
16. Kremers GJ, Goedhart J, van Munster EB and Gadella TW. Cyan and yellow super fluorescent proteins with improved brightness, protein folding, and FRET Förster radius. Biochemistry 2006, 45: 6570–6580.
17. Goedhart J, van Weeren L, Hink MA, Vischer NO, Jalink K and Gadella TW. Bright cyan fluorescent protein variants identified by fluorescence lifetime screening. Nat Methods 2010, 7: 137–139.
18. Markwardt ML, Kremers GJ, Kraft CA, Ray K, Cranfill PJ, Wilson KA and Day RN, *et al*. An improved cerulean fluorescent protein with enhanced brightness and reduced reversible photoswitching. PloS ONE 2011, 6: e17896.
19. Goedhart J, von Stetten D, Noirclerc-Savoye M, Lelimousin M, Joosen L, Hink MA and van Weeren L, *et al*. Structure-guided evolution of cyan fluorescent proteins towards a quantum yield of 93%. Nat Commun 2012, 3: 751.
20. Chu J, Haynes RD, Corbel SY, Li P, González-González E, Burg JS and Ataie NJ, *et al*. Non-invasive intravital imaging of cellular differentiation with a bright red-excitable fluorescent protein. Nat Methods 2014, 11: 572–578.
21. Strongin DE, Bevis B, Khuong N, Downing ME, Strack RL, Sundaram K and Glick BS, *et al*. Structural rearrangements near the chromophore influence the maturation speed and brightness of DsRed variants. Protein Eng Des Sel 2007, 20: 525–534.
22. Niwa H, Inouye S, Hirano T, Matsuno T, Kojima S, Kubota M and Ohashi M, *et al*. Chemical nature of the light emitter of the Aequorea green fluorescent protein. Proc Natl Acad Sci USA 1996, 93: 13617–13622.
23. Patterson GH, Knobel SM, Sharif WD, Kain SR and Piston DW. Use of the green fluorescent protein and its mutants in quantitative fluorescence microscopy. Biophys J 1997, 73: 2782–2790.